Nuclear Materials and Energy 38 (2024) 101600

Contents lists available at ScienceDirect

Nuclear Materials and Energy

journal homepage: www.elsevier.com/locate/nme

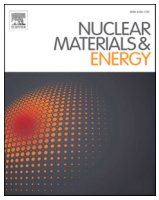

Ab-initio simulations of atomic hydrogen interaction with Nb and V at clean and oxygen covered surfaces

Alejandro Vazquez Cortes [a,b,*], Christian Day [a], Christopher Stihl [a], Pavel V. Vladimirov [a]

[a] Karlsruhe Institute of Technology, Karlsruhe, Germany
[b] Departamento de Física, Universidad Carlos III de Madrid, Leganés, Spain

ARTICLE INFO

Keywords:
Superpermeation
MFP
Niobium
Vanadium
VASP
Hydrogen
Oxygen monolayer

ABSTRACT

Superpermeation allows for hydrogen fluxes through metal foil membranes at rates orders of magnitude higher than pressure driven permeation. This process occurs only for hydrogen isotopes, meaning it is hydrogen-selective, and it can work against a pressure gradient, implying pumping capabilities. These characteristics allow for using superpermeation as the base process for a very efficient, selective separation of hydrogen from other gases.

However, the efficacy of superpermeation needs further research both experimentally and theoretically. Its efficiency relies on a surface energetic barrier that hinders both adsorption of molecular hydrogen on the downstream side and desorption on the upstream side, while leaving atomic hydrogen absorption unaffected. Such a barrier can be created by a monolayer of non-metallic impurities (usually oxygen) that naturally develops at group 5 metal surfaces. The physics explaining why such a monolayer drastically affects atomic hydrogen reactions are being explored in this work via density functional theory (DFT) calculations for the implementation of which we use the Vienna ab-initio Simulations Package (VASP).

By performing structural relaxations and saddle point-searching calculations deploying a dimer method using VASP, energy diagrams for atomic hydrogen absorption are obtained for two representative materials, namely niobium and vanadium. The differences in these diagrams are analyzed and compared in order to determine which material is optimal for superpermeation. To that end, slabs with (1 0 0) surface orientation are compared for the case with and without an O monolayer coverage. The characteristic energies involved according to the diagrams and the types of absorption sites will be key parameters to understand and, eventually, optimize for the emerging phenomena. It was found that the presence of an oxygen monolayer is necessary of superpermeation to occur, and that for the 100 orientation, the vanadium system provides better characteristics.

1. Introduction

The current global economic trends towards a green economy with the electrification and hydrogenation of industrial processes are inevitable in view of global climate change. The purification and separation of hydrogen from other gases in mixed streams is one of the technological challenges for the hydrogen energetics.

Such separation at low pressure can be carried out via superpermeation through metal foils, and a very specific feature of them is the ability of energetic hydrogen to superpermeate through them. This is an effect identified by its name first in [1]; later Peters provided a detailed review of previous results in [2], along with a review in depth of the different individual processes involved. This effect allows for perfectly selective separation of hydrogen isotopes from other gases and this process can even work against a pressure gradient.

In typical pressure driven hydrogen permeation, the molecules should overcome an adsorption energy barrier to undergo a dissociative adsorption to a metal surface to form two hydrogen atoms before they can be absorbed into the bulk. Whilst for superpermeation, hydrogen in form of atoms, protons or molecular ions is attracted by the surface. As far as these hydrogen forms are produced by a plasma source or a gas ionizer, they are referred to as “hot” or “suprathermal” in contrast to the thermalized gas of hydrogen molecules named “thermal molecule”. This nomenclature is due to the higher energy these particles have in comparison with the thermal molecules.

The suprathermal hydrogen approaches the metal surface without an

* Corresponding author.
E-mail address: alejandro.cortes@kit.edu (A. Vazquez Cortes).

https://doi.org/10.1016/j.nme.2024.101600
Received 1 August 2023; Received in revised form 22 January 2024; Accepted 25 January 2024
Available online 1 February 2024

energy barrier for its adsorption and is therefore absorbed into the metal membrane with significantly higher probabilities than the thermal hydrogen [1,3]. However, the membrane material should have an energy barrier for desorption at the surface facing the suprathermal hydrogen (upstream) to reduce probability of associative desorption, as shown in Fig. 1. This barrier may emerge, for instance, due to the presence of non-metal impurities at the surface thus inhibiting the surface thermal reactions of the molecular hydrogen (both recombination and dissociation). This effectively reduces the molecular sticking and recombination coefficients [1,4]. However, the suprathermal hydrogen does not confront with such difficulties because the process does not have a dissociation barrier (pink line in Fig. 1), and its energy is higher than the barrier energy for atomic absorption ($E_{r0,L}$). Thus, the flux from suprathermal hydrogen remains unaffected by this barrier. Due to the reduction of the recombination coefficient, the hydrogen atoms in the bulk cannot easily escape back through the upstream surface and thus diffuse in a random-walk process downstream (characterised by diffusion energy E_D and enthalpy of solution ΔH), where they recombine and desorb as a molecule. If there were only a barrier upstream, virtually all the absorbed hydrogen could recombine and desorb at the downstream surface. In a real case scenario, a barrier appears at both sides, and they are usually almost symmetric. The latter means that half of the absorbed hydrogen is desorbed downstream and the other half is released upstream [2] resulting in the 50 % efficacy of hydrogen permeation.

Taking the previous considerations into account, it can be stated that the optimal characteristics for the superpermeability of a material are a low diffusion energy in order to strengthen the bulk diffusion and keep the process in the surface limited regime, and a high energy barrier between the surface and the bulk so that the hydrogen back-permeation towards upstream is hindered.

The main potential application for superpermeation is the separation of unburnt hydrogen fuel (DT) from exhaust gases in fusion reactors such as DEMO, a concept called 'Direct Internal Recycling' [5]. A similar concept was already proposed for ITER by Livshits in [6], but not implemented there. The Direct Internal Recycling concept reduces the total tritium inventory and meets the more severe requirements of a DEMO machine compared to ITER [7,8]. The primary technology choice for this separation is called Metal Foil Pump (MFP) [9], which is part of the proposed technical realization of the Direct Internal Recycling concept [10]. The current design of a MFP consists of a collisional plasma line that energizes the hydrogen isotopes, providing them with enough energy to be implanted under the surface of a group 5 metal (Nb or V) membrane to initiate the superpermeation process [11]. The foreseen MFP plasma source has a much higher yield of atomization than ionization. Based on the literature review and experimental studies of different materials including, e.g., V, Nb, Fe, stainless steel and Cu [2] two major candidates, namely Nb and V, are considered for this simulation study.

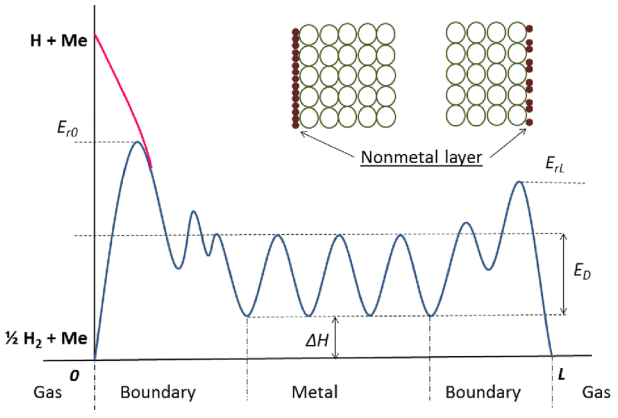

Fig. 1. Generic H absorption path diagram in realistic metal slab surface.

Superpermeation has been extensively studied in experiments with different membrane materials and suprathermal hydrogen sources [12–16]. However, simulations of hydrogen atom interaction with group 5 metals surfaces at the atomic scale are still scarce. There are some reports on simulation of clean surfaces [17], of other groups' metals [18] or just a study of the behaviour of the surface impurities [19], but no work on group 5 metals covered by non-metal impurities to the authors' knowledge was published. Providing the first ab-initio studies of the atomic hydrogen interactions with and beneath Nb and V surfaces covered by O monolayer and producing an absorption path energy diagram are the main goals of the present work.

2. Simulation methods

In order to accomplish this task, the Vienna Ab-initio Simulation Package (VASP) [22,23] was chosen as simulation tool to carry out density functional theory (DFT) based calculations for identification of stable hydrogen adsorption sites at surfaces and interstitial sites in the bulk, as well as its diffusion pathways. To that end, Perdew-Burke-Ernzerhof (PBE) generalised gradient approximation functional [24] was used to treat the electronic exchange and correlation and the projected augmented wave method (PAW) [25] was employed in order to deal with the electronic core. Nb is a group 5 transition metal, which was considered as an ion with 11 free electrons (valance and semi-core) as a reasonable trade-off between accuracy and computational complexity ($4p^6\ 5\ s^1\ 4d^4$), while V was considered as an ion with 5 free electrons for the same reason ($3d^4\ 4\ s^1$). The kinetic cut-off energy of the plane wave basis set was 360 eV for Nb and 380 eV for V. The Brillouin zone sampling was carried out with a resolution of $2\pi \cdot 0.14$ Å^{-1} for Nb and $2\pi \cdot 0.16$ Å^{-1} for V, resulting in a consistent 5x5x1 grid for both sets of calculations. These values were chosen from a parametric study of the energy difference per atom so that the delta energy per atom and the absolute energy contribution per atom, respectively, were smaller than 10^{-3} eV, as shown in Figs. 2 and 3. Fermi level smearing was applied via the ISMEAR- and SIGMA-tags, where a first order Methfessel-Paxton method with a broadening of 0.2 eV was found to result in negligible entropy terms. Regarding structural optimization, electronic convergence was assumed based on an energy difference less than 10^{-6} eV and a force-based ionic convergence criterion was set to 10^{-2} eV/Å. For the search of transition state configurations between stable sites, i.e. saddle points, the dimer method as implemented in the VTST patch set [26] is employed. In order to ensure sufficiently accurate forces to facilitate necessary finite difference evaluations a significantly lower energy difference convergence tolerance (10^{-7} eV) was chosen.

The initial bcc unit cells used to build the surfaces were taken from

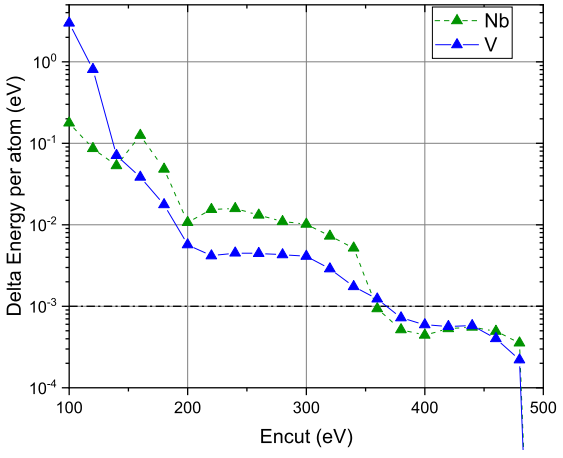

Fig. 2. Parametric study of encut accuracy for Nb (dashed green) and V (solid blue). (For interpretation of the references to colour in this figure legend, the reader is referred to the web version of this article.)

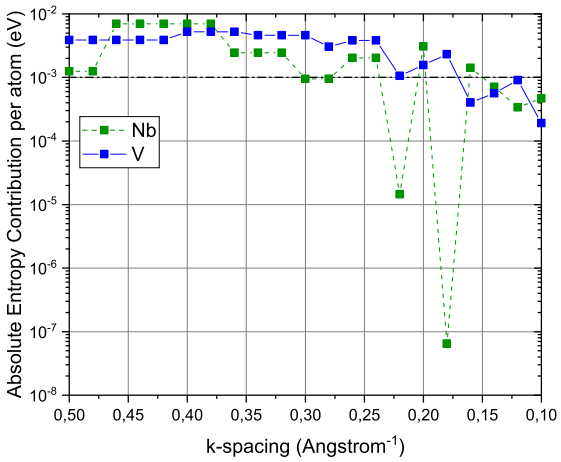

Fig. 3. Parametric study of k-spacing accuracy for Nb (dashed green) and V (solid blue). (For interpretation of the references to colour in this figure legend, the reader is referred to the web version of this article.)

[27] (material ID mp-146 for V, with a 2.98 Å lattice constant and mp-75 for Nb, with 3.32 Å). The simulation supercell consists of a slab of 144 metal atoms (WidthxHeightxLength = 3x3x16 positions) and one hydrogen atom at various interstitial positions as it permeates through the slab. Nine oxygen atoms were added in the case of the presence of O surface coverage. The bottom 4 layers of the slab are frozen and the remaining 12 can freely relax in all three directions, the vacuum region is nearly 50 Å thick for Nb and 32 Å thick for V, due to the smaller size of its unit cell. This initial configuration was cut from a fully relaxed 24 layers slab so that the mid layers experience a relative change in their mutual distances of less than 0.1 % with respect to their initial configuration.

For the calculation of the absorption energies, the following procedure is carried out. Firstly, a relaxation of the metal slab without the H atom is performed (yielding the total energy E_{met}). Separately, a hydrogen molecule is also relaxed (resulting in the total energy E_{H2}). These two energy values are used as references for the calculation of the system's energy with one H atom at various positions. According to literature, the most stable interstitial site for hydrogen in both metals is the tetrahedral interstitial site (T), being more preferable than the octahedral one (O) [28]. Therefore, these sites were taken as the initial guess for stable configurations near surface. For the subsurface and surface, the T-like was preferred, although the results on the stability in those areas of Qin et al. for V [29] and Ferrin et al. for Ta (as reference hint for Nb) [17] were also taken into account. The results of Gong [19] and Hua [30] for V were used as references for both metals because of their chemical similarity for the initial position of the O atoms on the (1 0 0) surfaces, on the hollow surface sites (HS). As a visual example, Fig. 4 shows a bcc metal with a (1 0 0) oriented surface (surface atoms in dark green and first subsurface atoms in light green) with the O atoms (in red) at the HS. Both V and Nb have bcc structure, so the difference in their visual representation would be just the distance between the atoms.

Once the initial stable sites for the H are selected, the slab is structurally optimized and its energy $E_{met,H}$ obtained. The energy of the slab system with one H atom at a certain position is thus given by equation (1):

$$E^{H}_{met} = E_{met,H} - E_{met} - \frac{1}{2}E_{H2} \quad (1)$$

During searches for saddle point configurations (SP) using the dimer method, the initial positions of the atoms are given by the linear interpolation between two adjacent stable T sites, and the initial direction of the dimer is along the vector connecting the two atomic configurations.

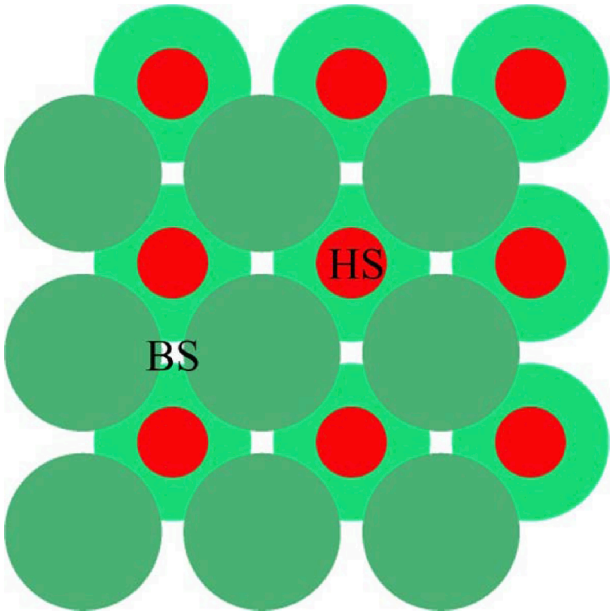

Fig. 4. Bcc metal (1 0 0) oriented surface with O atoms at the HS.

The choice to employ the dimer method over other common transitional state strategies, such as climbing image-Nudge Elastic Band (CI-NEB) comes from the fact that contrary to the CI-NEB method, which needs 'known' reactants and products, the dimer only requires an initial state and a direction of search. This characteristic allows to find transitional states that might have stayed undetected.

In addition, if the disturbance of the surface atoms due to the presence of the H is large (indicated by a sudden drop in the calculated energy), E_{met} is updated as the energy of that configuration relaxed without the H atom. Zero-point energies are neglected throughout this paper because Qin showed in [28] that its inclusion does not change the type of preferential interstitial sites, which metal has higher or lower solution enthalpies or diffusion barrier within the group 5 metal-hydrogen system.

In this first of a kind study of threefold interaction (metal, O and H), the (1 0 0) orientation was chosen. Even though there is experimental evidence of (1 0 0) surface reconstruction in the presence of O atoms in bcc metals [20,21], a possible reason for the lack of surface reconstruction observed in these calculations is the reduced surface area of the simulation (3x3 unit cells). The size of the reported superstructures are 5x1 in V [21] and 3x1 in Nb [20]. Thus, the proximity of the supercell periodic boundaries may prevent a free surface reconstruction. Future publications will employ larger surface areas to bring this effect to light.

3. Results

All the energy absorption path diagrams shown in this section have the same structure. The z-position of the H atom (in Å) and the reaction coordinate with respect to the coordinate of the topmost metal atom in the slab are used to identify the different interstitial hydrogen positions. The reaction coordinate is calculated as the distance of the displacements along the path of all the system atoms normalized by the sum of the differences in positions of all the atoms at the two minima. The energy of the system (in eV) is calculated via equation (1). The bulk-like part of the plot contains the information about the migration energy and the enthalpy of solution, the surface part about the surface adsorption sites, and the subsurface (in light blue shade) part represents the transition behaviour from bulk to surface due to larger lattice distortions and the change in the charge distribution caused by the proximity of vacuum. For the sake of clarity we have subdivided all absorption paths into surface, subsurface and bulk-like regions. This subdivision is based

solely on the changes in the corresponding energy profiles. The surface domain includes only adsorption sites, i.e. those with the positive H z-coordinates. The bulk-like behaviour is characterized by constant migration barriers, while the intermediate region in between the two is called subsurface in the following.

The H absorption path energy diagrams described in this section allow to derive the most important characteristic energies for H transport. They are defined as the energies of the system that can be easily identified in all cases and that are useful to characterise the super-permeation process. Each of the three regions contains these characteristic energies.

3.1. Clean V slab with (100) surface

The absorption path energy diagram for atomic hydrogen in V with a (100) clean surface is given in Fig. 5. It is clearly seen that the stable sites in the subsurface area have higher energies than in the bulk and the surface sites. A higher energy means that staying in the subsurface area is less energetically favourable for the H than moving to the bulk or to the surface sites, thus making the hydrogen dissolution in V exothermic. The most stable surface site was found to be a HS, as expected for V [17]. In addition, the energy of the outer bridge site (BS), shown in Fig. 4, was also calculated for completeness. In the bulk, it is observed that the distance in the normal direction to the surface between Ts is constant. This is because the jumps between Ts always have the same angle with respect to (100).

3.2. Monolayer O coverage on V slab with (100) surface

Fig. 6 shows the absorption path energy diagram of H on a (100) V surface with an O monolayer coverage. As expected, the bulk area largely resembles the bulk of the clean (100) V surface diagram, since the surface state should not alter the bulk properties, although the calculated migration energies are slightly lower. The increase of dissolution energies in the subsurface part compared to the bulk is a common feature with the clean (100) V, acting as an obstacle to the hydrogen diffusion to the surface from the bulk. Comparison of clean and oxidized surfaces suggests that the overall height of the barrier to overcome this zone is nearly independent of surface oxidation. On the other hand, the main differences begin close to the surface, where the distance along surface normal between Ts decreases remarkably, as indicated in the H z-coordinate axis. A large energetic barrier that appears in the subsurface (0.64 eV towards surface, 0.87 eV towards bulk) is not due to the H displacement (although in the plot the horizontal H movement is not represented), but to the shift of the O surface atoms. A second even

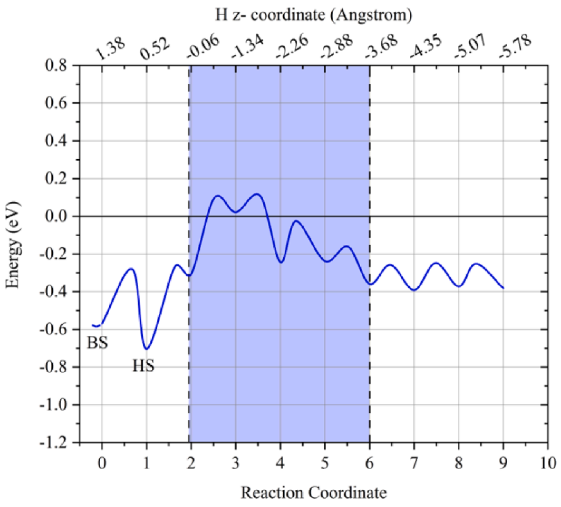

Fig. 5. Atomic hydrogen absorption path diagram for clean 100 surface of V.

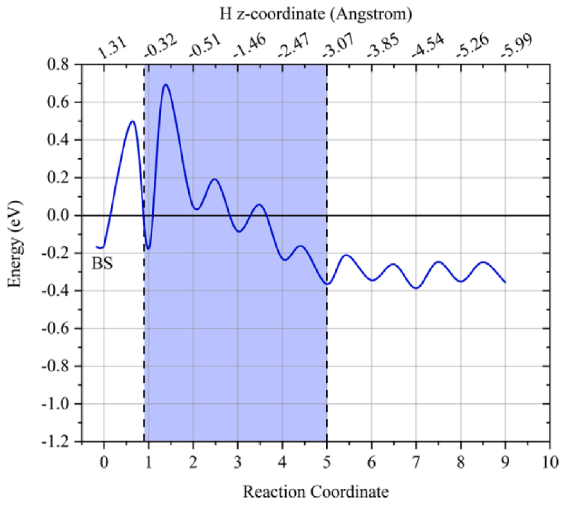

Fig. 6. Atomic hydrogen absorption path diagram for 100 surface of V with O monolayer coverage.

larger energy barrier at the limit between the only found stable surface site connected to the diffusion path (a BS) and the subsurface region appears (exact values in Table 1). The energy of the BS on the oxidized surface is higher than the energy for the BS on the clean surface.

3.3. Clean Nb slab with (100) surface

Fig. 7 displays the absorption path energy diagram of H in clean Nb slab with a (100) surface. As well as in V, the subsurface Ts have larger energies than the bulk and the surface sites. Our simulations show that the BS is a more stable site for H adsorption than HS is for clean (100) Nb slab. This finding is contrary to the results from [31], which reports on Mo-doped and pure Nb (100) surfaces. The difference in the stability of the sites comes probably from the fact that the surface to subsurface path selected in [31] is different from the one presented in this work, even in the case of pure Nb. The permeation path outlined in this work is more probable because of our application of the dimer method for the calculation of the migration barrier instead of the CI-NEB method applied in [31], which assumes an initial and final reaction states when searching for transitional states. In this material, the distance between Ts is longer than in V due to the larger lattice constant of Nb.

3.4. Monolayer O coverage on Nb slab with (100) surface

Fig. 8 shows the absorption path energy diagram of H on a (100) Nb surface with an O monolayer coverage. As in the V case, the bulk area is expected to largely resemble the bulk of the (100) clean Nb surface diagram, since the surface state should not affect the bulk properties. The irregularities in the horizontal distances between SPs and Ts shown in the plot come from the choice of the reaction coordinate as the

Table 1
Characteristic energies.

	Clean V	O covered V	Clean Nb	O covered Nb
Enthalpy of solution	−0.40 eV	−0.37 eV	−0.41 eV	−0.42 eV
Migration Energy	0.13 eV	0.08 eV	0.15 eV	0.16 eV
Surface site(s) energy	BS: −0.57 eV HS: −0.70 eV	BS: −0,16 eV	BS: −0.64 eV HS: −0.47 eV	HS: −0.31 eV
Surface-subsurface barrier	0.46 eV	0.66 eV	0.26 eV	0.23 eV
Subsurface-surface barrier	0.04 eV	0.68 eV	0.05 eV	0.28 eV

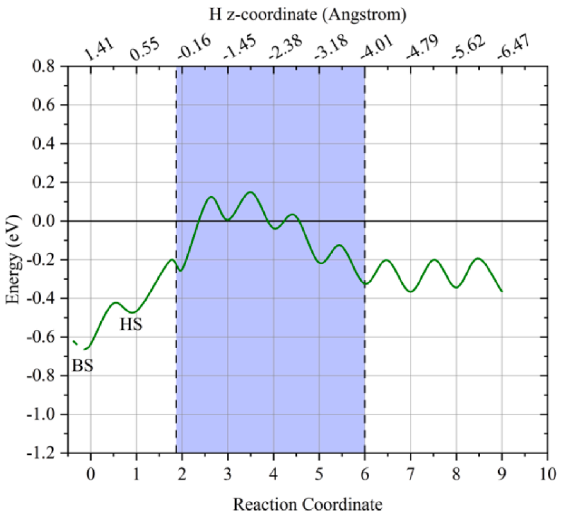

Fig. 7. Atomic hydrogen absorption path diagram for clean 100 surface of Nb.

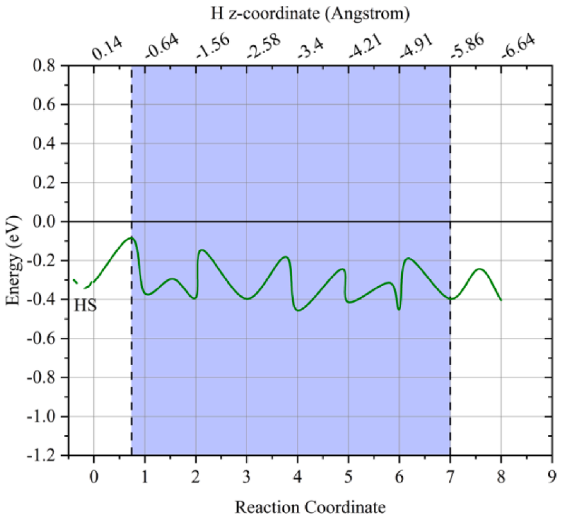

Fig. 8. Atomic hydrogen absorption path diagram for 100 surface of Nb with O monolayer coverage.

abscissa the energies are plotted against. The z-coordinate of the H atom is also displayed in order to illustrate that the displacement of the H atom is indeed regular. In order to illustrate this, let us consider the H displacement between reaction coordinates 5 and 6. While the position of the SP is clearly asymmetric when plotted against the reaction coordinates, its position is fairly symmetric when plotted against the H atom z-coordinate (see complementary files). For instance, this indicates that in the case of the H traveling from 6 to 5, firstly the H moves to the SP position and then the surrounding lattice follows these late displacements are responsible for the observed asymmetry. The differences in energies again can be found in the subsurface area, where the energies of the Ts are lower in the slab with O coverage. However, the most remarkable discrepancy is a single energy barrier before entering the surface area. In this case, only one stable surface site connected with the permeation path was found as well. This was a HS, contrary to the V case, in which the stable surface site was a BS.

4. Discussion

Firstly, from the bulk part of the diagrams the enthalpy of H solution and the migration energy for interstitial H diffusion can be retrieved. At the surface, the hydrogen energy at the adsorption sites is representative of the site's stability. The lower the energy, the more stable such configuration is. In the subsurface area, the energies of the migration barrier from the lowest surface site to the top subsurface site and vice versa indicate how likely it is for the H atom to move in respective direction. Table 1 provides a list of these characteristic energies for the four investigated cases.

As expected, the characteristics from the bulk are very similar for each individual material, regardless of whether the slab contains an oxygen monolayer or not. The main differences are in the migration energies. They are probably due to the inclusion of O atoms in the simulation setup, which are distorting the charge distribution near the surface, or the effect of the vacuum volume, which allows for large displacements of the lattice atoms (disturbing the system too much). Even taking into account these perturbations, both parameters in the four cases are in plausible agreement with literature values for calculations in the bulk of material [28,30] and T enthalpy of solution calculations in an identical geometry as in [28] (-0.36 eV in the case of V and −0.37 eV in the case of Nb).

On the other hand, the near-surface parts of the energy diagram are remarkably diverse. The stable surface sites for H adsorption in clean slabs with a (100) surface have 2 (for BS) or 5 (for HS) metal atom neighbours. These configurations are displayed in Fig. 9. Even though both sites are stable for H adsorption (the energy after adsorption is lower than before, resulting in energy gain), the most stable sites for V and Nb are different. In the former, the most stable site is the HS, while in the latter, it is the BS. The similarity between the Nb surface-H interactions obtained in this work and the Ta results from [17] indicates that Nb is more similar to Ta than to V with respect to H absorption.

In the case of the Nb with O monolayer coverage, H partially displaces O atom off the HS and occupies its place to a certain extent. For V

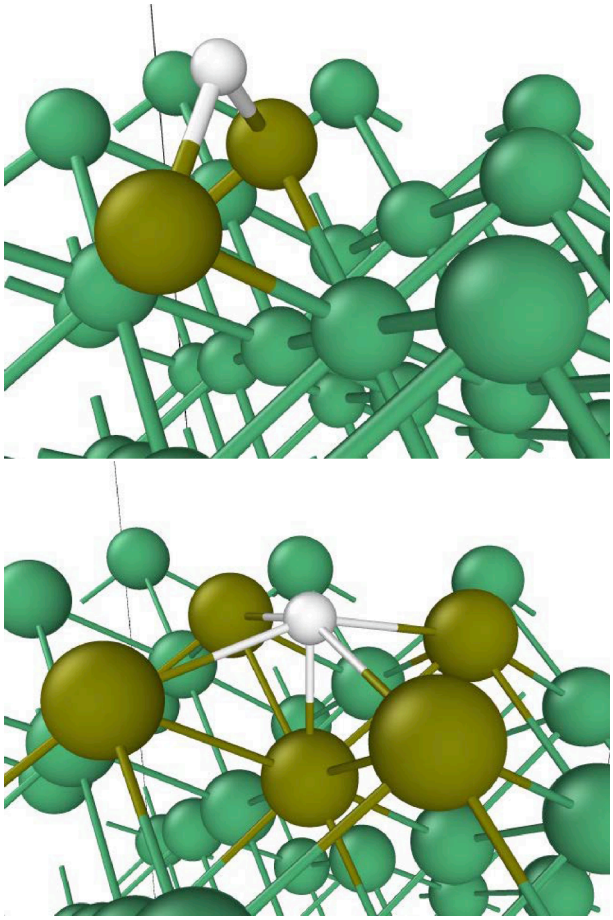

Fig. 9. (100) bcc metal surface BS (top) and HS (bottom) surface sites [32].

with O coverage, on the other hand, the H atom occupies preferentially a BS, barely displacing the O atoms. Although they are disturbed in the process of the H crossing the monolayer. The Nb HS is more stable than the V BS.

The analysis of the subsurface regions is more cumbersome. In the cases of clean surfaces and the O covered V, the energy of the stable subsurface sites is higher than in bulk and surface, indicating the need of extra energy to move through this area. The amount of necessary energy changes depending on the material, and the presence of O monolayer reduces it in the case of Nb. In fact, the most striking difference appears when O is present at the surface, since energy barriers appear for both materials, hindering the jump of one H atom from the surface sites to the subsurface and vice versa. This barrier is the cause of the reduction of adsorbed H flow from surface to subsurface and vice versa, effectively translating into reduction of the molecular surface reaction coefficients (sticking and recombination) in practice.

The most remarkable formal difference between Nb and V with O coverage is the presence of a second subsurface barrier in V. This barrier emerges from large displacements of the O surface atoms to accommodate the H at a new position. The lack of this second barrier in Nb can come from the difference in chemical interactions of Nb and V with oxygen atoms. The difference in energy barrier sizes is also remarkable, being much lower for Nb.

5. Conclusions

The performed DFT ab-initio studies of the H absorption path energy diagrams for different Nb and V surface conditions allow to assess which conditions would be beneficial for superpermeability. The desirable characteristics of a material for optimal superpermeability are low migration energy to enhance diffusion and to keep the process surface limited, and a high barrier between the surface and the bulk in order to inhibit H backward movement of hydrogen to surface sites on the upstream side.

As expected, the diffusion barrier height is very similar for Nb with and without O monolayer, as well as the solution enthalpy. The V results show larger differences, indicating that the presence of O affects to deeper layers in V.

The size and shape of the subsurface-surface barrier depends highly on the surface state. For instance, the clean Nb has lower barriers because the top subsurface site is almost at the same vertical position as the surface Nb atoms. The heights of the barriers are 0.26 eV for surface to subsurface transition and 0.05 eV for the move backwards. Nevertheless, the most interesting case is with O monolayer coverage. In the case of oxidised Nb, a barrier of 0.28 eV blocks the back-permeation of H towards the surface, while a 0.23 eV barrier blocks the absorption from the surface sites. This indicates that H absorption by the O monolayer is slightly more favourable than the backward movement leading eventually to desorption on the upstream side.

The clean V surface has a lower barrier as well for the same reasons as in the Nb case (0.46 eV and 0.04 eV), although its location is deeper due to the larger stability of the HS. The case of V with O coverage shows a higher barrier inhibiting the absorption from the surface sites than Nb (0.66 eV). The barrier blocking the back-permeation is also higher (0.68 eV).

To summarize, it has been shown that the migration energy of V is comparable to the one of Nb (0.13 eV vs. 0.15 eV). Furthermore, it has been found for the oxygen covered cases that the surface–subsurface and vice versa barriers are practically equal for the two metals, but at different levels (about factor 3 higher in the case of V). The barrier height inhibiting the back-permeation of H by preventing the H atoms to move into the surface sites is clearly larger for V. On the other hand, Nb has a lower barrier from the surface. This could allow for H atoms with lower energies to enter the subsurface.

The oxygen monolayer described in this work arises naturally in vacuum in group 5 metals at high temperatures [13]. If the monolayer of one side of the membrane is damaged via e.g. sputtering, oxygen dissolved in the bulk can replenish it in order to keep the oxygen surface coverage symmetric under the proper conditions [33]. The possibility to coat one of the surfaces in order to, for instance, reduce the downstream barrier, presents challenges associated to the metallic inter-diffusion [34].

Therefore, it can be stated that the O monolayer is indispensable for superpermeability to be feasible for both materials. Because of the higher energy barrier hampering hydrogen from reaching external surfaces, the low index V surface seems to have better properties regarding the surface–subsurface transition and bulk diffusion than Nb. However, the absorption energies and behaviour can change dramatically in high index surfaces compared to low index ones [35]. Thus, in order to confirm the advantages of V over Nb as a superpermeable membrane, further studies of higher index surfaces are needed.

It is also worth mentioning that the energetics here described would apply only to a low H coverage case, when there are barely interactions between H atoms. In order to take these interactions into account, larger simulation cells would have to be employed. On the one hand, the H atom would not influence itself as it permeates, and on the other, more different hydrogen coverages could be considered. With the estimation of the energetics of the high coverage cases, a rate equation model could be constructed. This path will be followed in future publications. In addition, the employment of larger simulations cells would allow to take into consideration possible surface reconstructions as well, without the risk of the superstructure formation being influence by itself due to the proximity of the periodic boundaries.

Finally, it would be desirable to check if the behaviour of the other hydrogen isotopes is much different from that of protium via the evaluation of Zero Point Energy, similarly as was done in [36].

CRediT authorship contribution statement

Alejandro Vazquez Cortes: Writing – review & editing, Writing – original draft, Visualization, Investigation, Formal analysis, Data curation, Conceptualization. **Christian Day:** Writing – review & editing, Resources, Project administration, Funding acquisition. **Christopher Stihl:** Writing – review & editing, Validation, Software, Methodology.

Declaration of competing interest

The authors declare that they have no known competing financial interests or personal relationships that could have appeared to influence the work reported in this paper.

Data availability

Data will be made available on request.

Acknowledgments

Calculations presented here were carried out on the EUROfusion high performance computer (HPC) Marconi, under the project MFP_KIT. This work has been carried out within the framework of the EUROfusion Consortium, funded by the European Union via the Euratom Research and Training Programme (Grant Agreement No 101052200 — EUROfusion). Views and opinions expressed are however those of the author (s) only and do not necessarily reflect those of the European Union or the European Commission. Neither the European Union nor the European Commission can be held responsible for them.

We acknowledge support by the KIT-Publication Fund of the Karlsruhe Institute of Technology.

Appendix A. Supplementary data

Supplementary data to this article can be found online at https://doi.

org/10.1016/j.nme.2024.101600.

References

[1] A.I. Livshits, et al., Physico-chemical origin of superpermeability – Large-scale effects of surface chemistry on "hot hydrogen permeation and absorption in metals, J. Nucl. Mater. 170 (1990) 79–94, https://doi.org/10.1016/0022-3115(90)90329-L.

[2] B.J. Peters, Development of a hydrogen-selective vacuum pump on the basis of superpermeation, PhD-thesis, karlsruhe institute of technology Karlsruhe. (2020), https://doi.org/10.5445/IR/1000122305.

[3] A.I. Livshits, et al., Plasma driven superpermeation of hydrogen through group Va metals, J. Appl. Phys. 84 (5) (1998) 2558–2564. https://ui.adsabs.harvard.edu/link_gateway/1998JAP....84.2558L/doi:10.1063/1.368418.

[4] A.I. Livshits, et al., Large-scale effects of H_2O and O_2 on the absorption and permeation in Nb of energetic hydrogen particles, J. Nucl. Mater. 178 (1991) 1–18, https://doi.org/10.1016/0022-3115(91)90450-L.

[5] C. Day, et al., The direct internal recycling concept to simplify the fuel cycle of a fusion power plant, Fusion Eng. Des. 88 (2013) 616–620, https://doi.org/10.1016/j.fusengdes.2013.05.026.

[6] A.I. Livshits, et al., Superpermeability: critical points for applications in fusion, J. Nucl. Mater. 220–222 (1995) 259–263, https://doi.org/10.1016/0022-3115(94)00424-2.

[7] C. Day, et al., A smart three-loop fuel cycle architecture for DEMO, Fusion Eng. Des. 146B (2019) 2462–2468, https://doi.org/10.1016/j.fusengdes.2019.04.019.

[8] B.J. Peters, et al., Metal foil pump performance aspects in view of the implementation of direct internal recycling for future fusion fuel cycles, Fusion Eng. Des. 136 (2018) 1467–1471, https://doi.org/10.1016/j.fusengdes.2018.05.036.

[9] C. Day, et al., Development of advanced exhaust pumping technology for a DT fusion power plant, IEEE Trans. Plasma Sci. 42 (4) (2014) 1058–1071, https://doi.org/10.1109/TPS.2014.2307435.

[10] T. Giegerich, C. Day, The KALPUREX-process – A new vacuum pumping process for exhaust gases in fusion power plants, Fusion Eng. Des. (2014), https://doi.org/10.1016/j.fusengdes.2014.03.082.

[11] S. Hanke, et al., Progress of the R&D programme to develop a metal foil pump for DEMO, Fusion Eng. Des. 161 (2020) 111890, https://doi.org/10.1016/j.fusengdes.2020.111890.

[12] H. Hackfort, et al., Hydrogen pumping and compression by superpermeation through iron, J. Nucl. Mater. 144 (1987) l0–l, https://doi.org/10.1016/0022-3115(87)90273-X.

[13] Y. Hatano, et al., Influence of oxygen and carbon on performance of superpermeable membranes, Fusion Eng. Des. 81 (2006) 771–776, https://doi.org/10.1016/j.fusengdes.2005.06.368.

[14] R.K. Musyaev, A.A. Yukhimchuk, B.S. Lebedev, A.O. Busnyuk, M.E. Notkin, A. A. Samartsev, A.I. Livshits, Study of hydrogen isotopes superpermeation through vanadium membrane on "Prometheus" setup, Fusion Sci. Technol. 54 (2) (2008) 523–525, https://doi.org/10.13182/FST08-A1868.

[15] J. Park, et al., Permeation of hydrogen through palladium, J. Nucl. Mater. 220–222 (1995) 827–831, https://doi.org/10.1016/0022-3115(94)00591-5.

[16] B.J. Peters, C. Day, Analysis of low pressure hydrogen separation from fusion exhaust gases by the means of superpermeability, Fusion Eng. Des. 124 (2017) 696–699, https://doi.org/10.1016/j.fusengdes.2017.05.124.

[17] P. Ferrin, et al., Hydrogen adsorption, absorption and diffusion on and in transition metal surfaces: a DFT study, Surf. Sci. 606 (2012) 679–689, https://doi.org/10.1016/j.susc.2011.12.017.

[18] Y. Li, et al., Enhanced diffusion and permeation of hydrogen species on the partially carbon covered iron surfaces, Appl. Surf. Sci. 515 (2020) 145899, https://doi.org/10.1016/j.apsusc.2020.145899.

[19] L. Gong, et al., The stability and diffusion properties of foreign impurity atoms on the surface and in the bulk of vanadium: a first-principles study, Comput. Mater. Sci. 81 (2014) 191–198, https://doi.org/10.1016/j.commatsci.2013.08.011.

[20] A.A. McMillan, et al., A combined helium atom scattering and density-functional theory study of the Nb(100) surface oxide reconstruction: phonon band structures and vibrational dynamics, J. Chem. Phys. 156 (2022) 124702, https://doi.org/10.1063/5.0085653.

[21] R. Koller, et al., The structure of the oxygen induced (1x5) reconstruction of V (100), Surf. Sci. 480 (2001) 11–44, https://doi.org/10.1016/S0039-6028(01)00978-5.

[22] G. Kresse, J. Furthmüller, Efficient iterative schemes for ab initio total-energy calculations using a plane-wave basis set, Phys. Rev. B. 54 (1996) 11169, https://doi.org/10.1103/PhysRevB.54.11169.

[23] G. Kresse, D. Joubert, From ultrasoft pseudopotentials to the projector augmented-wave method, Phys. Rev. 59 (1999) 1758, https://doi.org/10.1103/PhysRevB.59.1758.

[24] J.P. Perdew, et al., Accurate and simple analytic representation of the electron-gas correlation energy, Phys. Rev. B. 45 (23) (1992) 13244–13248, https://doi.org/10.1103/physrevb.45.13244.

[25] J.P. Perdew, et al., Generalized gradient approximation made simple, Phys. Rev. Lett. 77 (18) (1996) 3865–3868, https://doi.org/10.1103/PhysRevLett.77.3865.

[26] G. Henkelman, et al., A dimer method for finding saddle points on high dimensional potential surfaces using only first derivatives, J. Chem. Phys. 111 (15) (1999) 7010–7022, https://doi.org/10.1063/1.480097.

[27] A. Jain*, S.P. Ong*, G. Hautier, W. Chen, W.D. Richards, S. Dacek, S. Cholia, D. Gunter, D. Skinner, G. Ceder, K.A. Persson (*=equal contributions), The materials project: a materials genome approach to accelerating materials innovation APL, Mater. 1 (1) (2013) 011002.

[28] J. Quin, et al., Dissolution, diffusion, and penetration of H in the group VB metals investigated by first-principles method, Int. J. Hydrogen Energy, Int. J. Hydrogen Energy. (2019), https://doi.org/10.1016/j.ijhydene.2019.03.228.

[29] J. Qin, et al., Investigation of adsorption, dissociation, and diffusion properties of hydrogen on the V (1 0 0) surface and in the bulk: a first-principles calculation, J. Adv. Res. 21 (2020) 25–34, https://doi.org/10.1016/j.jare.2019.09.003.

[30] J. Hua et al., Effect of impurity carbon and oxygen atoms on the behavior of hydrogen in vanadium in a fusion environment: A first-principles study International Journal of Modern Physics B 32 21 2018 1850232 (13 pages) 10.1142/S0217979218502326.

[31] Y. Wu, et al., First-principles investigation of atomic hydrogen adsorption and diffusion on/into Mo-doped Nb (100) Surface, Appl. Sci. 8 (2018) 2466, https://doi.org/10.3390/app8122466.

[32] A. Stukowski, Visualization and analysis of atomistic simulation data with Ovito – the open visualization tool modelling simul, Mater. Sci. Eng. 18 (2010) 015012.

[33] A.I. Livshits, et al., Hydrogen superpermeation resistant to ion sputtering, Appl. Phys. A. 80 (1661–16669) (2005), https://doi.org/10.1007/s00339-004-2595-0.

[34] V.N. Alimov, et al., Hydrogen permeation through the Pd-Nb-Pd composite membrane: surface effects and thermal degradation, Int. J. Hydrogen Energy. 36 (2011) 7737–7746, https://doi.org/10.1016/j.ijhydene.2011.04.01.

[35] M. Lischka, et al., Hydrogen adsorption on an open metal surface: H2/Pd(210), Phys. Rev. B. 65 (2002) 075420, https://doi.org/10.1103/PhysRevB.65.075420.

[36] W. Setyawan, et al., Influence of hydrogen isotopes on vacancy formation and antisite defect diffusion in palladium and vanadium metals, Comput. Mater. Sci 197 (2021) 110641, https://doi.org/10.1016/j.commatsci.2021.110641.